ON THE USE OF SATELLITE INFORMATION TO DETECT COASTAL CHANGE: DEMONSTRATION CASE ON THE COAST OF SPAIN

Paula Gomes da Silva[1*]; Martínez Sánchez Jara[1], Raúl Medina[1], Anne-Laure Beck[2], Mohamed Amine Taji[2,3].

[1]IHCantabria – Instituto de Hidráulica Ambiental de la Universidad de Cantabria. C/Isabel Torres n°15 Parque Científico y Tecnológico de Cantabria 39011 Santander. Spain.

[2]Argans UK, 1 Davy Road, Plymouth Science Park, Derriford, Plymouth, PL6 8BX UK

[3]Geosciences Laboratory, Faculty of Sciences Ain Chock, University Hassan II, Casablanca 20100, Morocco

* Corresponding author. Tel.: +34 942 20 16 16.
E-mail address: gomesp@unican.es (P. Gomes da Silva).

Abstract

Recent developments in satellite processing tools allow noncost, fast and automatic processing of a large amount of information from Earth observation, enhancing the capability of detecting coastal changes from space at different temporal scales. However, these automatic procedures are usually based on processors calibrated with information from a limited set of beaches, and the application of these tools to areas with different conditions may lead to significant errors in coastal change assessment. In this work, we evaluate the capability to monitor changes in coastal morphology at various temporal and spatial scales using 1D (coastlines) and 3D (bathymetry) satellite-derived data obtained from site-specific processing methods. Local characteristics were included in several phases of the development of the satellite products used here: i) VHR images from each pilot site were used in the coregistration process to guarantee high geolocation accuracy in images from different missions, ii) different spectral indices were tested at each pilot site to guarantee reliable detection of the coastline at all sites and iii) measured topobathymetry data were used to obtain datum-based satellite shorelines and bathymetry. The accuracy and skill of those satellite products were assessed at several pilot sites in Spain. The results indicated high horizontal accuracy, with errors on the order of half of the pixel size. Time-series analysis using satellite-derived shorelines showed that coastal change processes can be detected at several temporal and spatial scales, such as short-term erosion and accretion events on a small beach, seasonal beach rotation, and long-term trends at local and regional scales. However, the results from satellite-derived bathymetry indicated that the quantitative assessment of the coastal morphology with 3D products is still limited. Some in situ measurements are necessary to obtain satellite data that represent site-specific conditions. However, the quantity of required data measured in situ is significantly lower than the quantity required by traditional monitoring methods.

Keywords: coastal morphodynamics, coastal erosion, coastal monitoring, Earth Observation, coregistration

1. INTRODUCTION

Sandy shores are highly dynamic areas affected by natural and human-induced changes that often put human assets and natural habitats located inland in the backshore area of erosion

hotspots at risk. Moreover, climate change is expected to intensify coastal erosion processes in the future and, consequently, aggravate coastal erosion impacts.

Regular and efficient monitoring is necessary to inform coastal management decisions, but although in situ measurements are highly efficient in capturing coastal features at a given time, the cost of continuous acquisition campaigns in large areas is dissuasive. In contrast, Earth observation, based on publicly available satellite missions equipped with optical sensors, provides wide spatial coverage over a large temporal scale at a reduced cost. Remarkably, the recent Sentinel-2 satellite provides a high temporal frequency (revisit time up to 2 days), and the earlier Landsat-5 and Landsat-8 provide a long temporal series (from 1984 to the present) (Turner et al., 2021).

The development of the Google Earth Engine (Gorelick et al., 2017) has made noncost satellite images available anywhere on the globe for the past 3 decades. Such a tool provides valuable data for analyzing coastal morphodynamics at local and global scales. Particularly at the global scale, recent studies with a high impact on the general media have been developed to assess erosion/accretion trends of the world's beaches based on the use of the Google Earth Engine to obtain massive satellite-derived data (Luijendijk et al., 2018; Vousdoukas et al., 2020a). Although these global assessments are undoubtedly relevant to providing an overall picture with regard to coastal change and to pinpointing critical erosion areas, they assume several simplifications, and the scientific community acknowledges the limitations of these kinds of approaches (Cooper et al., 2020; Vousdoukas et al., 2020b). The use of waterline processors for the automatic detection of instantaneous coastlines (e.g., Luijendijk et al., 2018; Vos et al., 2019b) is one of the simplifications of both global and local assessments based on globally available satellite-derived information. These processors are usually calibrated with information from a limited set of beaches, and consequently, the application of these tools to areas with different conditions may lead to significant errors in waterline detection and coastal change assessment (Castelle et al., 2021; Ceccon et al., 2021; Vos et al., 2019b)

In this work, we evaluate the capability to monitor changes in coastal morphology at various temporal and spatial scales, making use of satellite-derived data obtained from site-specific processing methods that were developed in the project "Coastal Erosion From Space" (https://coastalerosion.argans.co.uk/, hereafter, the CEFS project). For that purpose, the accuracy and skill of 1D and 3D satellite-derived products that represent the coastline and the seabed morphology have been assessed in several pilot sites in Spain with diverse geographical scopes from the local scale (i.e., a small beach) to the regional scale (i.e., a whole gulf), which

comprises 290 km of coast in total. At those sites, coastal changes were assessed in the short-term (i.e., erosion after a storm), midterm (i.e., seasonal beach rotation), and long-term (i.e., erosion due to chronic sediment deficits), taking advantage of the short revisit time of Sentinel-2 and long time series of Landsat-5 and 8.

2. STUDY SITES IN SPAIN

Four study sites were considered in this work (Figure 1): i) Malgrat Beach (1.5 km) located south of the Tordera River mouth in the Tordera Delta, ii) the beaches south of Barcelona located between Barcelona and Ginesta Ports (18 km), iii) the coastal stretch between the ports of Sagunto and Castellon (40 km) and iv) the Gulf of Cadiz between the Strait of Gibraltar and the Spanish-Portuguese border (230 km).

I. Malgrat Beach is located on the Spanish northern Mediterranean coast where the tidal range is lower than 1 m and extreme storm wave and surge events take place frequently (Sanuy and Jiménez, 2019). Rapid shoreline retreat over 25 m has been observed in Malgrat Beach after storm events (Jiménez et al., 2018), and this area has experienced a steady shoreline retreat of approximately 120 m over the past two decades, with erosion rates of approximately 3.8 m/year (Jiménez et al., 2011). We selected this site to assess coastal changes in the long- and short-term at a local scale.

II. The beaches south of Barcelona, with a marine climate similar to that of Malgrat Beach, are also located on the Spanish northern Mediterranean coast. The Llobregat River mouth is located in the northern part of El Prat Beach, where the sediment load of the river plume often causes high sediment and particulate matter concentrations in the water, which makes this area a challenge for detecting the seabed by optical sensors. Despite the sediment yield by the Llobregat River, long jetties on the river mouth and large breakwaters of Barcelona Port block littoral drift (from NE to SW) and cause erosion in the northern sector of these beaches (erosion rates up to 6 m/year were verified by Françoise et al., 2000), whereas the southern sector experiences accretion due to the accumulation of sediments at the main breakwater of Ginesta Port. To overcome the erosion problem, the Barcelona Port Authority backpasses the sediment once a year and undertakes a monitoring program that consists of topobathymetry field surveys before and after dredging and dumping operations in the borrow area (north of Port Ginesta) and dumping area (south of Barcelona Port). We selected this site to assess coastal changes due to human activities.

III. The coast between Castellon and Sagunto Ports, also located on the Spanish Mediterranean coast, is mostly urban with several artificial embayed beaches between man-made coastal structures. The tidal range in this area is microtidal, and the wave climate has a strong seasonal pattern, with dominant NE high waves during the winter and SE low-energy sea states during summer. The coastal configuration and the bimodal wave climate in the area cause a seasonal shoreline rotation, which is a process that has been reported previously on other beaches of the Spanish Mediterranean coast(e.g., Castelle et al., 2020; Ojeda and Guillén, 2008; Turki et al., 2013). We selected this site to investigate seasonal (midterm) coastal erosion patterns.

IV. Finally, the coast of the Gulf of Cadiz, with a tidal range of approximately 3 m, is located on the Spanish Southern Atlantic coast. Previous studies detected erosion hotspots at several locations in this area (CEDEX, 2013; MITECO, 2019). We selected this site to assess coastal change at a large scale.

This set of study sites was selected to evaluate the capability of satellite-derived data to detect coastal changes at several spatial and temporal scales. Furthermore, the set includes various environmental conditions (with regard to marine climate and tidal range) to challenge satellite-derived remote sensing skills, including sites with frequent cloud coverage or high concentrations of suspended sediment in the water column.

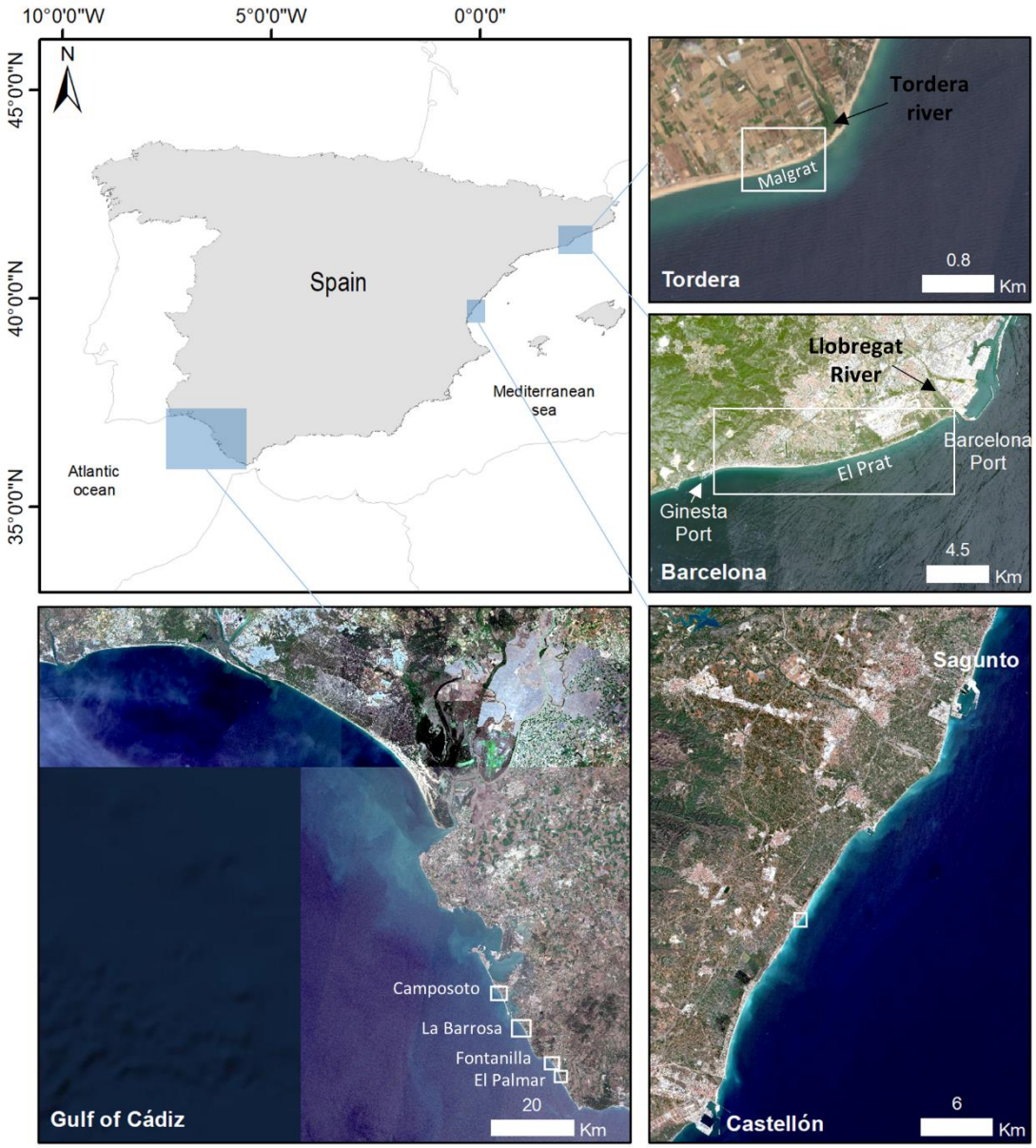

Figure 1: Pilot sites along the Spanish coast. The white squares highlight the areas used for the validation of satellite-derived products.

3. DATA

Diverse information can be extracted from satellite images to detect changes in coastal morphology, such as 1D coastlines (Vieira Da Silva et al., 2016; Vos et al., 2019a), 2D land cover maps (Ruiz-Luna and Berlanga-Robles, 2003), and 3D digital elevation models (Caballero and Stumpf, 2020, 2021; Erena et al., 2020). In this work, we focus on the changes detected by 1D and 3D products developed within the CEFS project that were obtained from Landsat-5, Landsat-8, and Sentinel-2 images (hereafter, CEFS products).

We validated the results obtained from the CEFS products (see Chapter 5), making use of in situ measurements (i.e., topobathymetric surveys) and reference data from previous scientific studies. In this chapter, we describe both the CEFS products and the validation dataset used in this work.

3.1. CEFS products

In regard to 1D products, detection of the coastline position in satellite images depends on the indicator used to determine the sea-land interface (e.g., the water-sand interface, the wet-dry sand interface, or the vegetation line – Ruggiero et al., 2003). The CEFS project developed two different 1D products that represent the coastline (*satellite-derived waterlines, SDW,* and *satellite-derived shorelines, SDS*) and one 3D product for the seabed morphology (*satellite-derived bathymetry, SDB*). Below, we briefly describe these three different products, which have been used in this work, and the auxiliary data (site-specific information) that enabled the development of such data (see Figure 2):

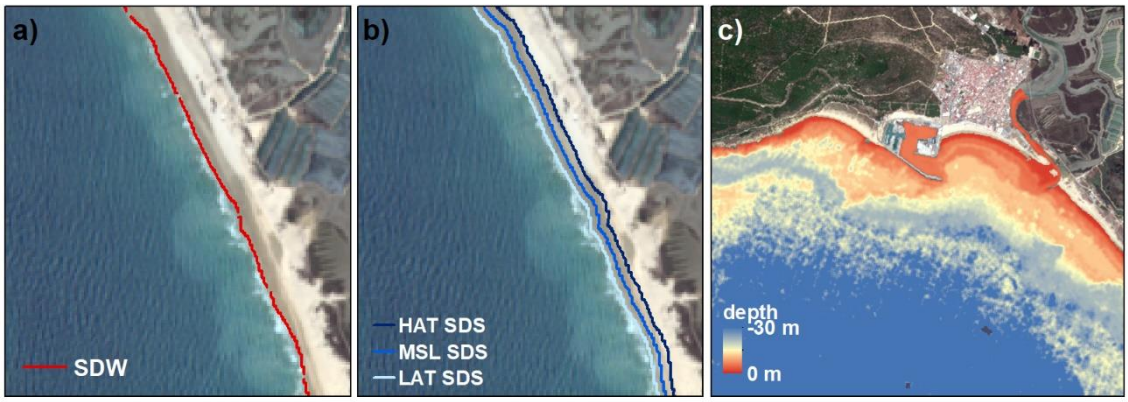

Figure 2: Examples of the three CEFS products: a) satellite-derived waterline (SDW), b) satellite-derived shoreline (SDS) and c) satellite-derived bathymetry (SDB). HAT is the highest astronomical tide, MSL is the mean sea level and LAT is the lowest astronomical tide.

- *Satellite-derived waterlines (SDW):* The satellite-derived waterline (Figure 2a) is the instantaneous interface between water and sand detected at the moment when the satellite image was taken, and it is associated with the water level at the same moment.
- *Satellite-derived shorelines (SDS):* The satellite-derived shorelines are datum-based lines derived from SDWs (Figure 2b). To detect changes over time, all waterlines must be referenced at the same water level (usually a local datum based on tidal records); otherwise, observed changes might come from changes in the water level and not from changes in coastal features. SDWs were transformed into SDSs to represent a certain datum. The correction was performed through trigonometric relations using the beach slope and water level measurements. Local beach topography from in situ surveys was

used to obtain the beach slope at each pilot site. The water level records were obtained from tide gauges of the national oceanographic monitoring system from *Puertos del Estado* (www.puertos.es). Water level reanalysis data from the Environmental Hydraulics Institute "IHCantabria" (Cid et al., 2014) were used where in situ measurements were not available.

- *Satellite-derived bathymetry (SDB):* Coastal bathymetry maps were developed from empirical relations between satellite spectral information and the depth of the water column. The result was digital elevation models in the submerged area. There are some limitations in the detection of satellite-derived bathymetry from optical sensors, and after completing all steps of SDB development, there was a significant reduction in the number of datasets in the time series when compared to the total number of images available.

This paper focuses on the capability of detecting coastal changes by means of satellite-derived data obtained from site-specific methods and not on the remote sensing processes applied to derive CEFS products from satellite images. Nevertheless, here, we highlight the three main innovative contributions of the processors to developing the SDWs, SDSs, and SDBs used in this work: i) coregistration of images, ii) locally adaptive waterline and shoreline extraction and iii) confidence indices associated with each product. These three innovations improve the *accuracy*, *precision,* and *reliability* of the CEFS products and are briefly explained below. Further details about the development of the SDWs, SDSs, and SDBs are available on the CEFS project website (https://coastalerosion.argans.co.uk/doc.html, see algorithm theoretical baseline documents).

3.1.1. Coregistration

When studying coastal change by means of several images in a time series, coregistration of images is key to guarantee that the observed coastal changes are not the result of differences in satellite sensors. In Landsat 8 images, the geolocation accuracy is approximately 30 m, while it is approximately 10 m for Sentinel-2 (L1C) (Clerc, 2021). The coregistration improves the *accuracy* of changes detected by satellite products, as it reduces that shift and guarantees the geolocation agreement between images from different sensors and with different spatial resolutions so that any feature in one image overlaps as well as possible its footprint in any other image in the time series.

The coregistration process applied to the CEFS products was carried out automatically, using very high-resolution commercial images as a reference (master images) to align the satellite images (slaves) (Figure 3a and Figure 3b). The structural similarity index measure (SSIM – Wang

et al., 2004), which indicates the similarity between images, increased significantly (ideal SSIM is 1) at all control points after coregistration was implemented (Figure 3c to Figure 3f). For the Tordera Delta, for example, 90% of the coregistered images showed horizontal and vertical shifts below 3 m in comparison to the master image (Gomes da Silva et al., 2020). To the author's knowledge, this is the first time that an automatic coregistration process has been applied to obtain coastal products such as waterlines, shorelines, and bathymetry.

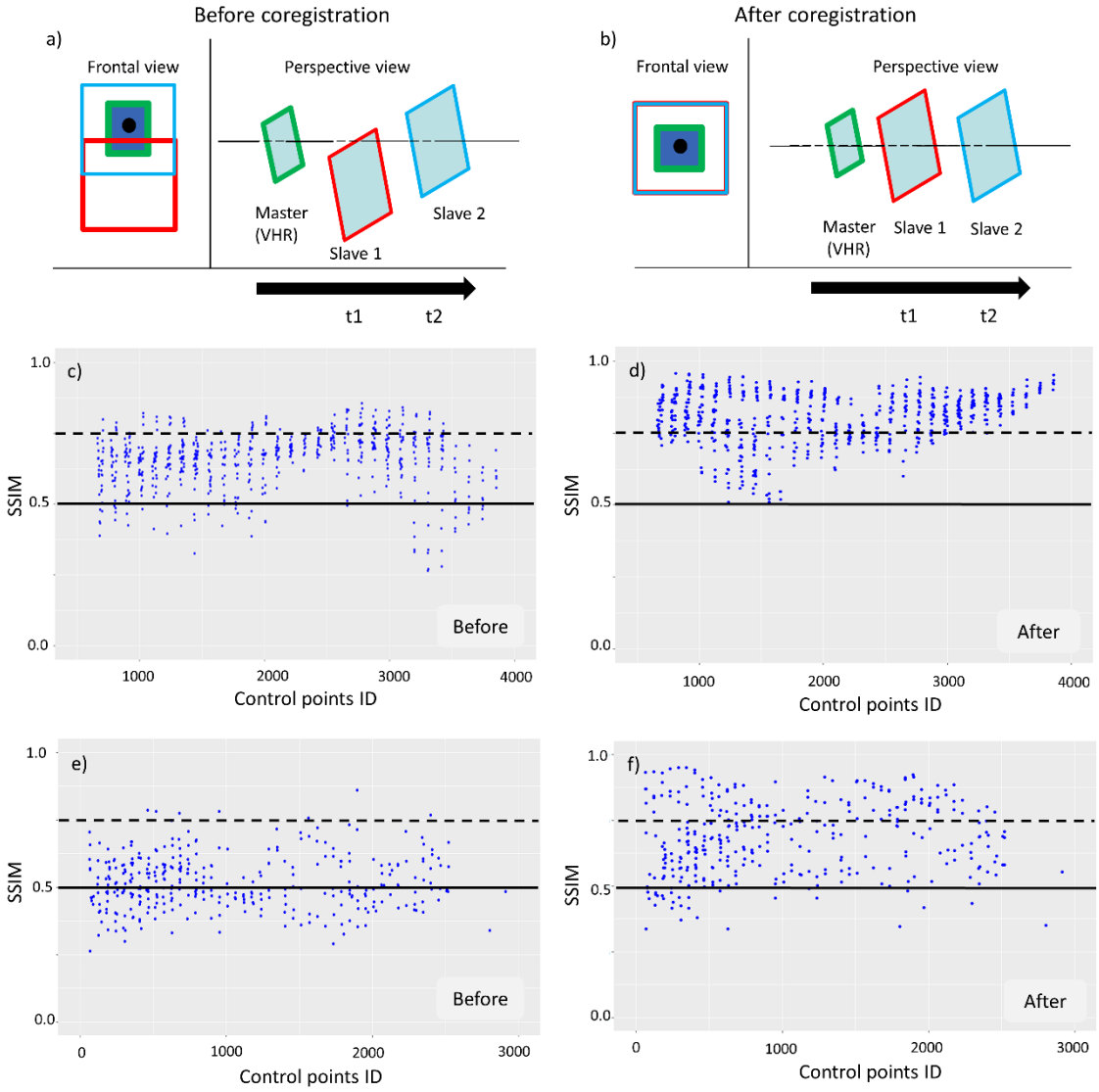

Figure 3: Scheme of the coregistration process (a and b) and SSIM results before and after coregistration on several control points of an image taken from Tordera (c and d) and Cadiz (e and f).

3.1.2. Waterline extraction

The satellite image resolution impacts the thickness of the interface between water and land, which represents the *precision* of the contour measurement, not to be confused with the *accuracy* of positioning the contour. There are subpixel methods to increase the resolution of satellite-derived data in an attempt to enhance their *accuracy*, but they were not applied to the

CEFS products. Instead, with regard to the positional *accuracy*, a coregistration method was implemented (see Section 3.1.1). For the *reliability* of the identification of the boundary between land and sea, the processing method to obtain SDWs included testing with different spectral indices to ensure the use of the best index at each pilot site. The spectral indices were used to obtain binary images in which the pixels were classified as water or land, which allowed the identification of the waterline as the border between those two classes. The normalized difference vegetation index (NDVI – Tarpley et al., 1984), the normalized difference water index (NDWI - Gao, 1996) and the green normalized difference vegetation index (GNDVI - Gitelson et al., 1996) were tested. A locally adaptive thresholding method on these spectral indices was designed according to the type of land cover and building on the established knowledge of the operator and the local specificities of the study locations. This includes site-specific information to the processor that improves waterline detection. Details about the methods applied to obtain site-specific SDW can be found in the algorithm theoretical baseline documents available at coastalerosion.argans.co.uk.

3.1.3. Datum-based shoreline

SDS vectors were developed by changing the SDW from its original water level (the water level at the moment that the image was taken) to a reference level using the typical beach slope and trigonometrical relations. Different proxies have been used to estimate the water level of CEFS waterlines depending on the available in situ measurements: the water level was either obtained from the nearest tide gauge or interpolated based on the Euclidean distances between nearby tide gauges if there was more than one (more details on site-specific SDS can be found in the algorithm theoretical baseline documents available at coastalerosion.argans.co.uk). This is particularly important for CEFS products developed at the regional scale, where relevant variations in the water level may exist along the pilot site. Preference was given to water levels obtained from in situ measurements, although reanalysis data were applied in those locations in which tide gauges were not available.

3.1.3. Confidence indices

Part of the limitations of satellite-derived data may be due to detection problems related to local environmental conditions and/or satellite instrumentation. Some examples of the environmental drivers of errors from the automated detection process are i) the presence of cloud cover, ii) suspended matter and sediment in the water column, iii) soil moisture (i.e., wet sand makes it difficult to detect waterlines during low tide) and iv) the presence of foam due to

wave breaking (Hagenaars et al., 2018). On the coast of Spain, all these drivers might occur individually or in combination, and satellite-derived data are frequently affected.

Confidence qualifiers were included within the metadata of all CEFS products to shed light on their *reliability*. Confidence indices of SDWs and SDSs were based on the occurrence of line vectors detected outside the typical area of waterlines and line vectors with lengths that did not agree with the coastal length. For example, this allows the detection of low confidence waterlines generated due to the presence of white water. Confidence indices of SDBs were based on the image reflectance, the amount of suspended matter, and the sediment concentration in the water column.

3.2. Validation data

The assessment of the accuracy of CEFS products and their ability to detect coastal change (see Chapter 4) require ground truth information based on either in situ measurements or reference data from previous works, as described below.

3.2.1. In situ measurements

Topobathymetry data from Malgrat Beach (Tordera Delta) measured on November 15th, 2015 are available. The beaches south of Barcelona have been monitored twice a year since 2007, and topobathymetric measurements have been carried out every pre- and postdredging operation by the port authority as part of a periodic sediment backpassing program. From those measurements, five dates matched the satellite-derived data from June 2015 to April 2018. Along the Gulf of Cadiz, in situ measurements are available at 4 different beaches: Camposoto, La Barrosa, El Palmar, and Fontanilla, from July 12th to July 16th, 2018 (see Figure 1).

Water level time series (including tide and storm surge variations) were obtained from the nearest tide gauges from *Puertos del Estado*. In situ waterlines were obtained from the available topobathymetry data and water level measurements. In this approach, the location of the measured waterline is the intersection between the terrain model and the water level. The water level at the moment when the satellite image was taken was estimated as the sum of astronomical tide and storm surge. The same procedure was applied to obtain the measured shorelines (datum based), applying the corresponding datum correction to the instantaneous water level.

3.2.2. Reference data from previous works

The reference data from previous works included i) trends in coastal evolution observed locally from in situ measurements and photogrammetry and ii) the erosion/accretion hotspots identified by the local authorities responsible for coastal protection. The works from Ojeda and Guillén (2008), Blasco (2011), Castelle et al. (2020), Turki et al. (2013), CEDEX (2013) and MITECO (2019) have been used as a reference for validation.

4. METHOD

The methodology to assess the ability of CEFS products to detect coastal changes can be divided into three steps: i) a visual check (see Section 4.1) to verify if the dataset from different missions is in accordance with the general aspects of the coast in each pilot site; ii) the accuracy assessment (see Section 4.2), based on differences between individual CEFS products and in situ measurements; and iii) the skill assessment (see Section 4.3), focused on the assessment of the ability of CEFS products time series to reflect coastal changes at different temporal and spatial scales.

4.1. Visual check

A qualitative by-eye check was performed to verify the consistency of CEFS products:

- SDWs should correspond to the water-sand interface in satellite images in the case of sandy coasts and the interface structure-water in the case of hard coasts.
- SDSs that represent different tidal levels should cover the totality of the intertidal area.
- SDBs should be coherent to typically known seabed morphology.

4.2. Accuracy assessment

The accuracy of CEFS products was assessed through the mean absolute error (MAE – Eq. 1) and the root mean squared error (RMSE - Eq. 2):

$$\boldsymbol{MAE} = \frac{\mathbf{1}}{\boldsymbol{N}}\sum_{\boldsymbol{j}=\mathbf{1}}^{\boldsymbol{N}}\left|\boldsymbol{x_j} - \boldsymbol{y_j}\right|, \quad (1)$$

$$\boldsymbol{RMSE} = \sqrt{\frac{\mathbf{1}}{\boldsymbol{N}}\sum_{\mathrm{j}=\mathbf{1}}^{\boldsymbol{N}}\left(\boldsymbol{x_j} - \boldsymbol{y_j}\right)^{\mathbf{2}}}, \quad (2)$$

where $\boldsymbol{x_j} - \boldsymbol{y_j}$ represents the error between in situ measurements and CEFS products (SDW, SDS, and SDB) and N is the number of pairs of data. The error position was quantified in terms of the cross-shore distance between coastlines extracted from in situ measurements and SDWs or SDSs over transects displayed every 20 m along the coast. For the bathymetry, the error was

298 estimated in terms of the difference in depth between in situ field surveys and the SDBs in points
299 distributed every 10 m over the target area.

300 The amount of data used in the accuracy analysis depends not only on the available CEFS
301 products but also on the availability of in situ measurements on similar dates. In this work, the
302 temporal distance between the time of satellite image acquisition and the date of in situ
303 measurements was limited to ensure the absence of significant morphological changes between
304 both datasets (see Table 1), and a maximum delay of ±6 days was accepted. A total of ten SDWs
305 (9 from Sentinel-2A and 1 from Landsat-8), ten SDSs, and three SDBs were assessed (only SDBs
306 that did not show inconsistencies due to sediment concentration were used). The absence of
307 concurrent in situ measurements with available CEFS products obtained from Landsat-5 does
308 not allow accuracy analysis of the dataset derived from this mission.

309 *Table 1: Dataset used to estimate the accuracy of satellite data from Landsat 8 (L8) and Sentinel 2 (S2).*

Site	In situ measurements	Satellite data (mission)
Malgrat Beach (Tordera)	11/Nov/2015	14/Nov/2015 (L8)
Barcelona	01/Jun/2016 (predredging)	07/Jun/2016 (S2)
	22/Jun/2016 (postdredging)	27/Jun/2016 (S2)
	23/May/2017 (predredging)	23/May/2017 (S2)
	13/Jun/2017 (postdredging)	12/Jun/2017 (S2)
	20/Apr/2018 (single measure)	18/Apr/2018 (S2)
Gulf of Cadiz (Camposoto)	12/Jul/2018	16/Jul/2018 (S2)
Gulf of Cadiz (Fontanilla)	13/Jul/2018	16/Jul/2018 (S2)
Gulf of Cadiz (La Barrosa)	16/Jul/2018	16/Jul/2018 (S2)
Gulf of Cadiz (El Palmar)	16/Jul/2018	16/Jul/2018 (S2)

310

311 **4.3. Skill assessment**

312 The ability of time series of CEFS products to detect changes on the coast was assessed in the
313 framework of several morphodynamic processes at diverse temporal and spatial scales (see
314 Table 2).

315 *Table 2: Dataset used to assess diverse coastal processes.*

Site	Coastal change process	CEFS products
Malgrat Beach (Tordera)	Long-term shoreline change	SDS time series (1995–2019)
	Pre- and postnourishment/erosion event	Pre- and postevent SDS
Barcelona	Changes in bathymetry	Pre- and postdredging SDB (2017)
Castellon-Sagunto	Seasonal beach rotation	SDS time series (2017-2018)

With regard to SDS, time series were compared to what was identified previously in the literature, and the following coastal change processes have been verified:

- Long-term SDS evolution trends were assessed on local (Malgrat Beach) and regional (Gulf of Cadiz) scales using the DSAS tool (Himmelstoss et al., 2018).
- Short-term SDS changes during specific events were assessed in Malgrat Beach through the analysis of the shorelines obtained immediately before and after nourishment and erosion events.
- Finally, SDS changes at the seasonal scale were assessed in three beaches on the coast between Castellon and Sagunto Ports.

For SDBs, their skill in detecting changes in the seabed was assessed through the Brier skill score (BSS - Sutherland et al., 2004), which is an estimate of the error relative to the changes observed in the ground and includes contributions due to errors in predicting amplitude, phase and mean. The BSS is calculated as:

$$\mathrm{BSS} = 1 - \frac{\frac{1}{N}\sum_{j=1}^{N}(x_j - y_j)^2}{\frac{1}{N}\sum_{j=1}^{N}(b_j - x_j)^2}, \quad (3)$$

where b_j is a baseline observation equal to the most likely anticipated change observed at the pilot site. Perfect agreement gives a skill score of 1, whereas observing the baseline condition gives a score of 0. SDBs obtained from 2017 in Barcelona were used in this analysis, and predredging in situ bathymetry was assumed to be the baseline for BSS estimation.

5. RESULTS

5.1. Visual check

The visual check of CEFS products aims to verify whether the detection process resulted in features that are coherent to what can be directly observed in the satellite images. The results of this visual check for 1D and 3D products are presented here.

5.1.1. SDW

In general, the SDWs agreed with the coastline shape in satellite images and represented both natural and human-made features well (Figure 4). The lines were distributed in the vicinity of port structures within a distance that visually agreed with image resolutions (Figure 4d). Natural

coasts were also well represented. Some stretches of the coast resulted in inconsistencies where the sediment plume or the foam resulting from wave breaking led to erroneous waterlines (foam and sediment plume were detected as land). In many cases, the confidence index values (see Section 3.1.3) available in the CEFS product metadata allowed the identification of those unreliable stretches, facilitating the visual check (Figure 5).

5.1.2. SDS

The SDSs correctly represented the expected tidal range observed in the various pilot sites with different tidal regimes. Natural and artificial coastlines were fairly represented as well (Figure 6).

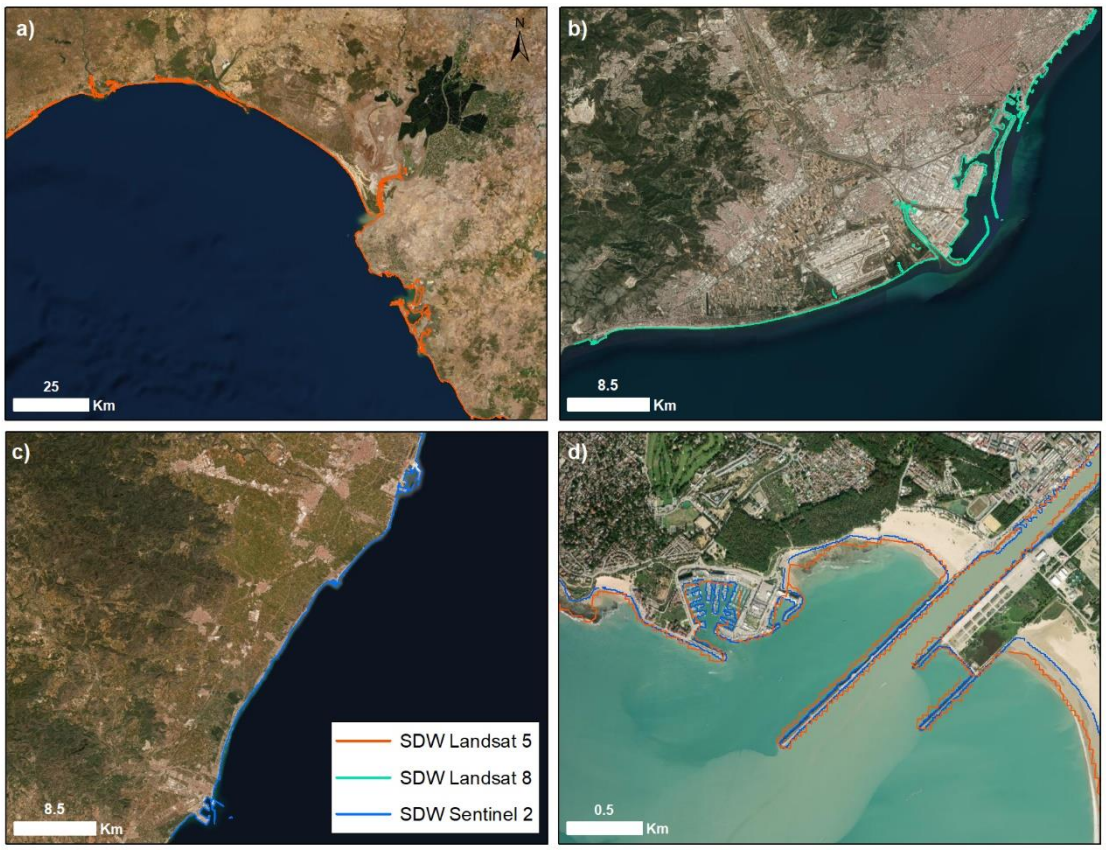

Figure 4: Examples of SDWs obtained from each pilot site. a) Landsat 5 SDW in the Gulf of Cadiz, b) Landsat 8 SDW in Barcelona and c) Sentinel 2 SDW in Castellon. d) Example of SDWs in ports.

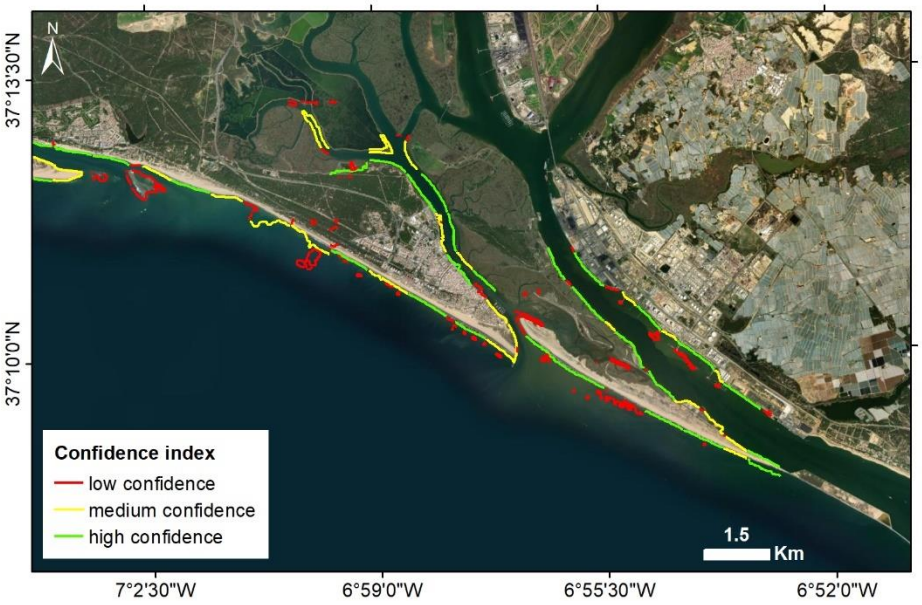

355

356 *Figure 5: Confidence index of an SDW from Huelva (Gulf of Cadiz).*

357

358 *Figure 6: Examples of SDSs from Castellon (left) and Cadiz (right). Tidal datums: lowest astronomical tide (LAT),*
359 *mean low water springs (MLWS), mean low water (MLW), mean sea level (MSL), mean high water (MHW), mean*
360 *high water spring (MHWS) and highest astronomical tide (HAT).*

361 *5.1.3. SDB*

362 The visual check of the SDBs indicated problems in conditions of high sediment concentration.
363 For example, some SDBs from Barcelona presented anomalous depth values after a strong river
364 discharge because the sediment plume was identified by the SDB algorithm as shallow waters

(Figure 7a and Figure 7b). When this type of condition takes place, the use of confidence indices (Figure 6c) allowed the identification of the SDBs that may contain erroneous information.

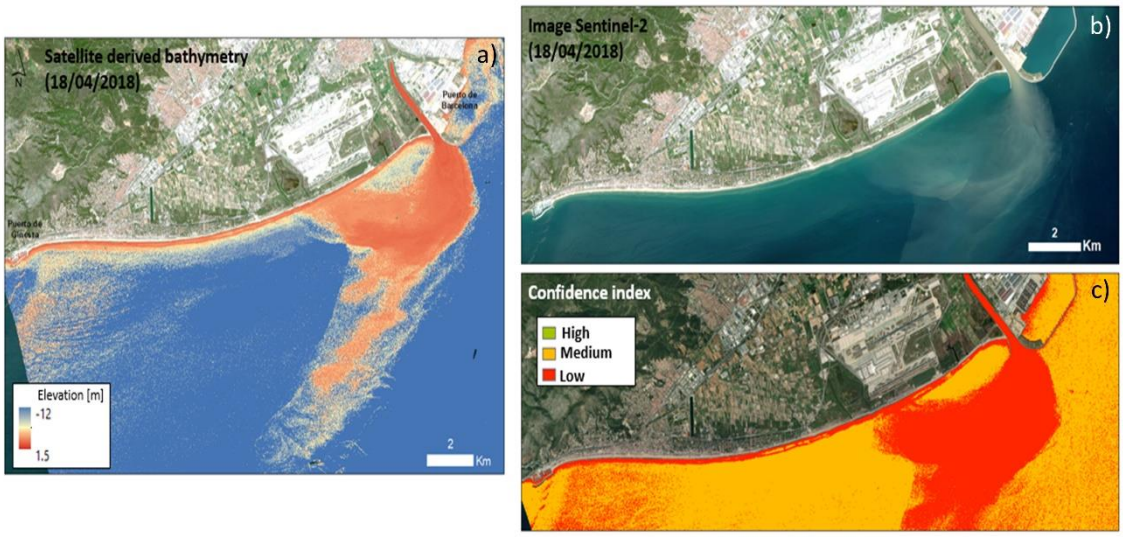

Figure 7: Example of inconsistencies observed in SDBs from Barcelona due to the sediment plume: a) SDB, b) satellite image from which the SDB was obtained, and c) confidence index.

5.2. Accuracy

The accuracy of 1D (SDW and SDS) and 3D (SDB) products were tested through RMSE and MAE statistics (Table 3), and details of the analysis are presented below.

Table 3: RMSE and MAE obtained from the analysis of the different CEFS products and from the different missions. h is the water depth.

CEFS products	RMSE [m] (Sentinel)	RMSE [m] (Landsat)	MAE [m] (Sentinel)	MAE [m] (Landsat)	BSS
SDW	8.4	15.3	5.8	14.7	-
SDS	9.1	18.9	5.6	18.4	-
SDB	1.13 (0.77 if $h^1 < 8$ m)	-	0.83 (0.63 if $h^1 < 8$ m)		0.26

[1]h=water depth

5.2.1. Accuracy 1D products (SDW and SDW)

The comparison between SDW and in situ measurements resulted in RMSE and MAE values below the pixel resolution of the satellite images from which the products were obtained (MAE and RMSE < 10 m for data from Sentinel 2 and < 30 m for data from Landsat 8) (see Table 3). As an example of the results at each study site, Figure 8 shows the distribution of the offset between the measured waterlines and SDWs at Barcelona, Tordera, and Fontanilla Beach (Gulf of Cadiz). These results represent the accuracy obtained from different missions (Sentinel 2 and

Landsat 8) and from diverse environmental conditions: the Mediterranean microtidal beaches of Barcelona and Tordera and Atlantic macrotidal Fontanilla Beach.

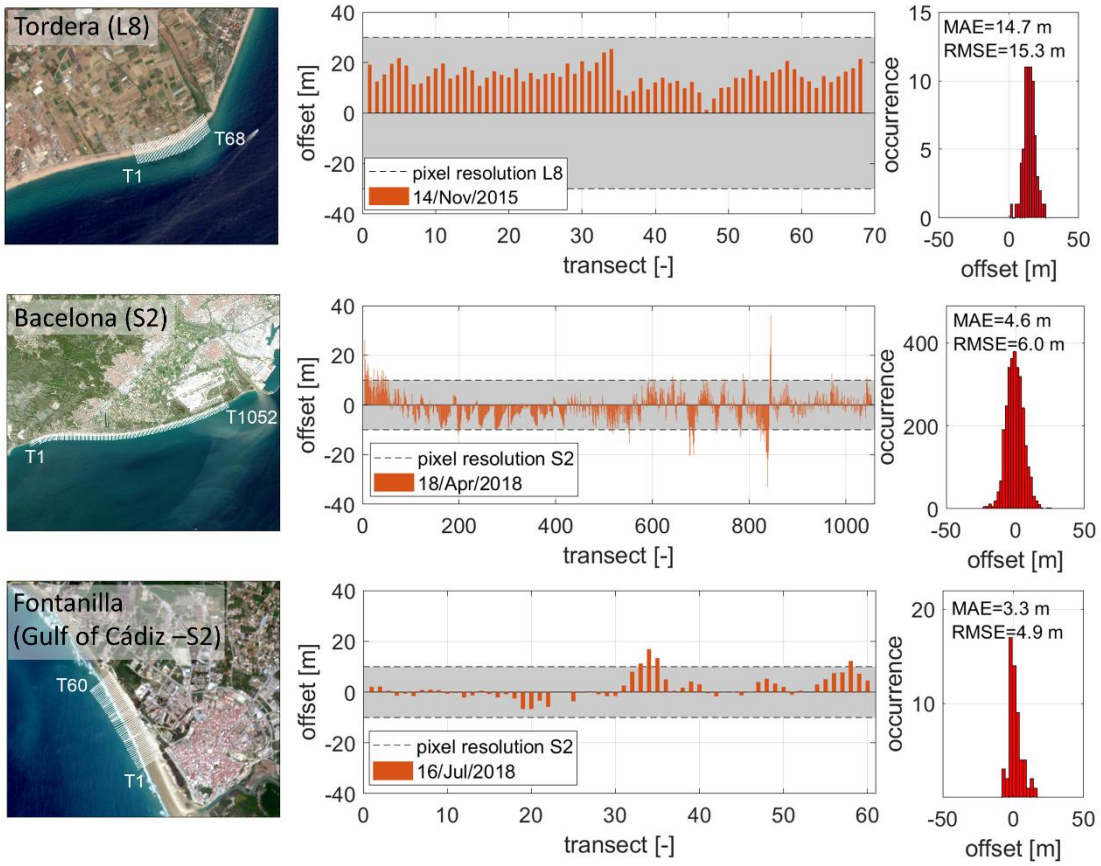

Figure 8: Examples of the accuracy results of SDW at a) Tordera (L8), b) Barcelona (S2) and c) Fontanilla – Gulf of Cadiz (S2). The left panels show the location of the transects at each beach, central panels present the offset per transect and right panels present the distribution of the offsets.

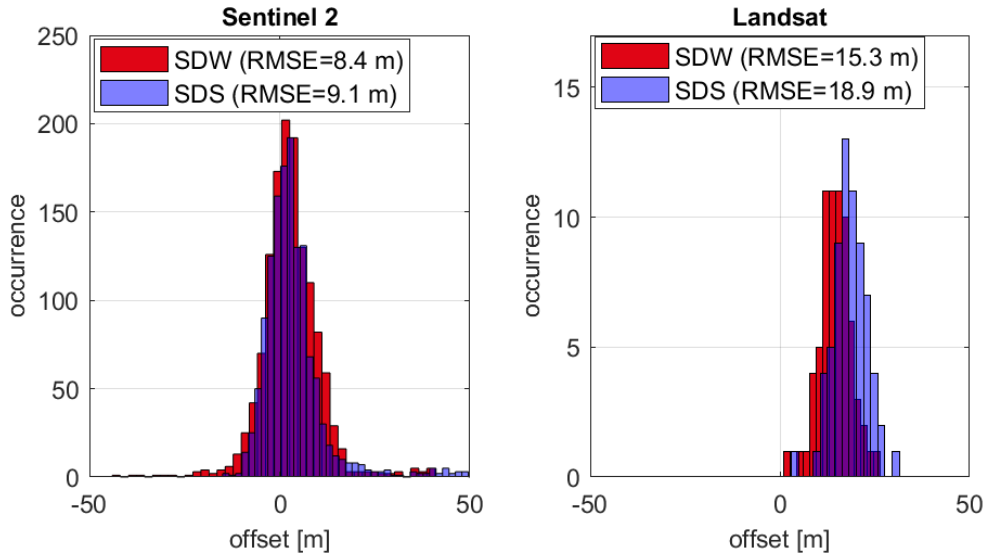

Figure 9: Overall accuracy of SDW and SDS: offset histograms from Sentinel 2 (left) and Landsat 8 (right). Positive (negative) offset values indicate that satellite data are located seaward (landward) from the measured line.

Some simplifications were assumed when developing those products, such as the use of a single slope to derive datum-based SDSs from SDWs that were applied irrespective of changes in the topography over time. Although the uncertainties related to this simplification add inaccuracies to the SDS (Figure 9), the MAE and RMSE values from the comparison between SDS and in situ measurements were in accordance with the pixel resolution of the satellite images (Table 3). It is worth noting that the purpose of transforming SDWs into SDSs was not to increase the accuracy of the individual products but to improve the coherence of the time series of products and, therefore, to improve the accuracy of the estimated changes.

5.2.2. Accuracy of 3D products (SDB)

A high correlation was observed between in situ measurements and SDBs, indicating the agreement between both sources of data. The majority of the dataset (84%) presented errors ranging between -1 and 1 m. The overall accuracy analysis of the three SDBs from the beaches of South Barcelona resulted in MAE and RMSE values equal to 0.83 m and 1.13 m, respectively (Figure 10a). Higher errors were observed at higher depths (see Figure 10c to Figure 10h), which highlights the limitation of the method used to estimate the bathymetry when applied to depths higher than 8 m (e.g., Yunus et al., 2019 found limitations in water depths > 10 m). By limiting the analysis to depths lower than 8 m, the MAE and RMSE were equal to 0.63 m and 0.77 m, respectively (not shown in the figure).

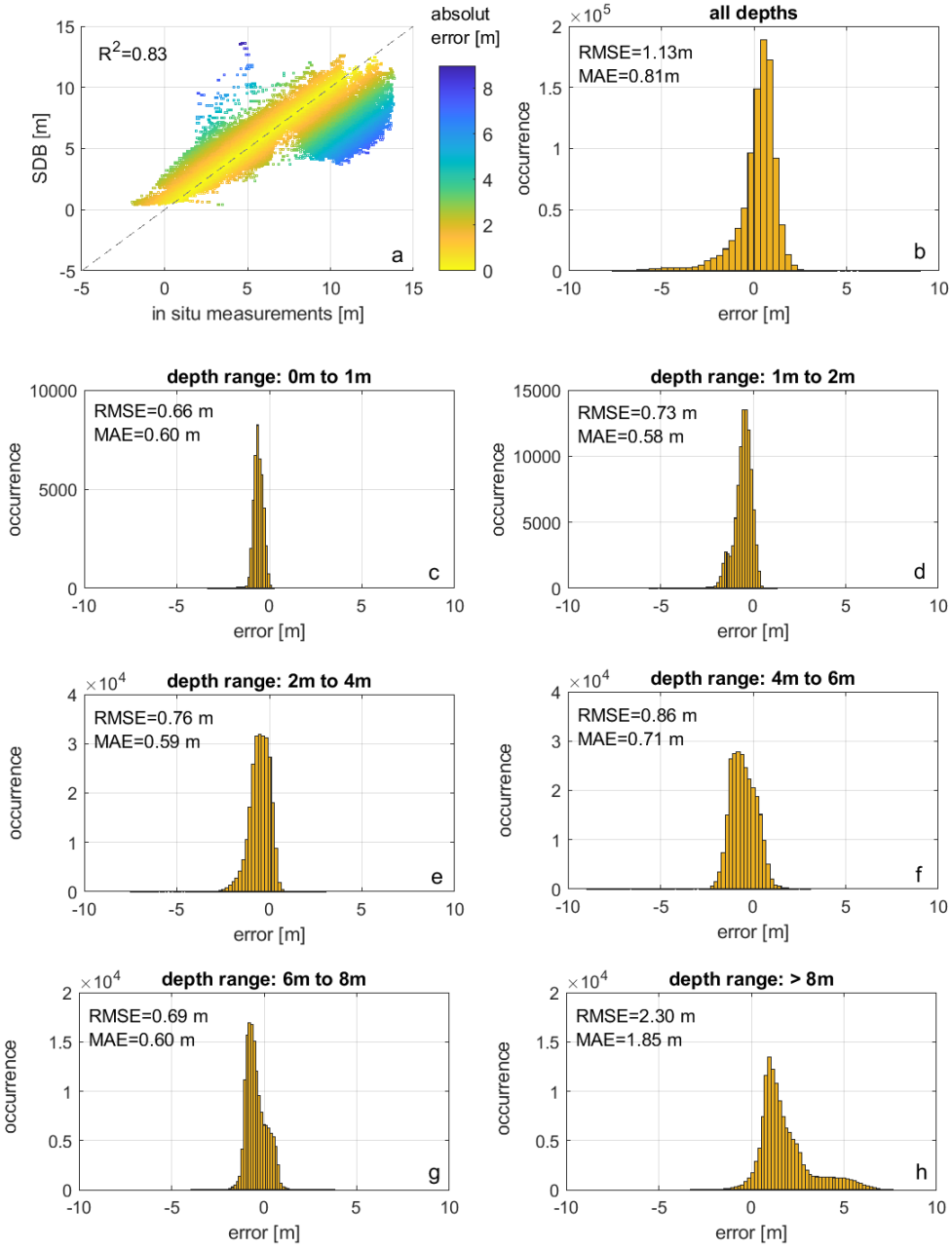

411

412 *Figure 10: Accuracy assessment of SDBs. a) Scatterplot between* in situ *measurements and SDB depths, b) distribution*
413 *of the error between both datasets, c) to h) distribution of the error obtained from different depth ranges.*

414 To verify whether SDBs can be used to identify seabed morphology, the dataset from 13th June
415 2017 (satellite) was compared to the data from 12th June 2017 (in situ). A longshore bar was
416 observed in both datasets (**¡Error! No se encuentra el origen de la referencia.** 11a and Figure
417 11b). Although the analysis showed a clear underestimation of depth values (Figure 11c) that
418 hampered the detection of temporal changes, both datasets presented similar bar shapes, and
419 the SDB was proven to be useful in terms of a qualitative assessment (Figure 11c).

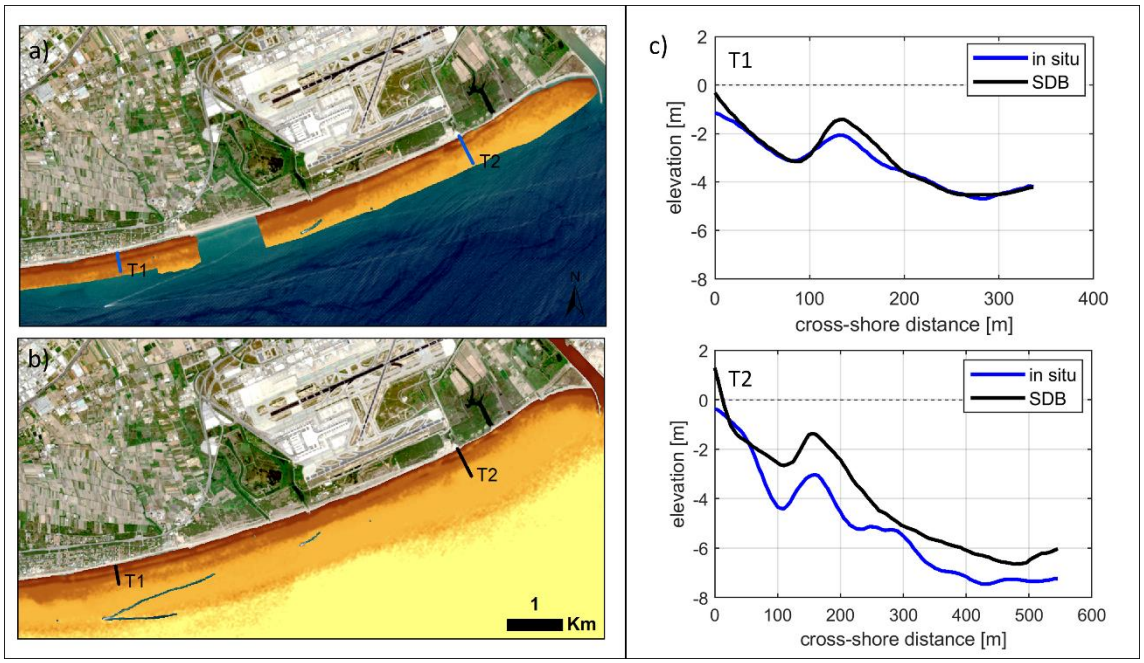

Figure 611: Identification of longshore bars in a) in situ *measurements and b) SDB and c) the cross-shore depth along transect T1 and transect T2.*

5.3. Skill

The skill of satellite data in reproducing coastal changes was tested through several study cases (see Table 2). The changes detected in each case are presented here, along with the assessment of the ability of CEFS products to showcase coastal changes at different temporal and spatial scales.

5.3.1. Long-term shoreline changes in Malgrat Beach (Tordera Delta)

A long-term analysis was carried out on Malgrat Beach using 24 years of shorelines (184 SDSs) along 68 cross-shore transects based on the cumulative shoreline movement and the resultant variation rate (calculated with a linear regression method). The analysis indicated a generalized erosion trend along the whole beach, with a minimum erosion rate of 2.5 m/year in the northern zone (transect 63 in Figure 12b) and a maximum erosion rate of 6 m/year in the central area (transect 33 in Figure 12b). This central area experienced a total retreat of almost 150 m in 24 years, and several campsites were affected by erosion due to both long-term processes and extreme storm events. In fact, all campsites seaward of the coastal road and some buildings had to be dismantled despite the rip-rap sea defenses (Figure 12c and Figure 12d).

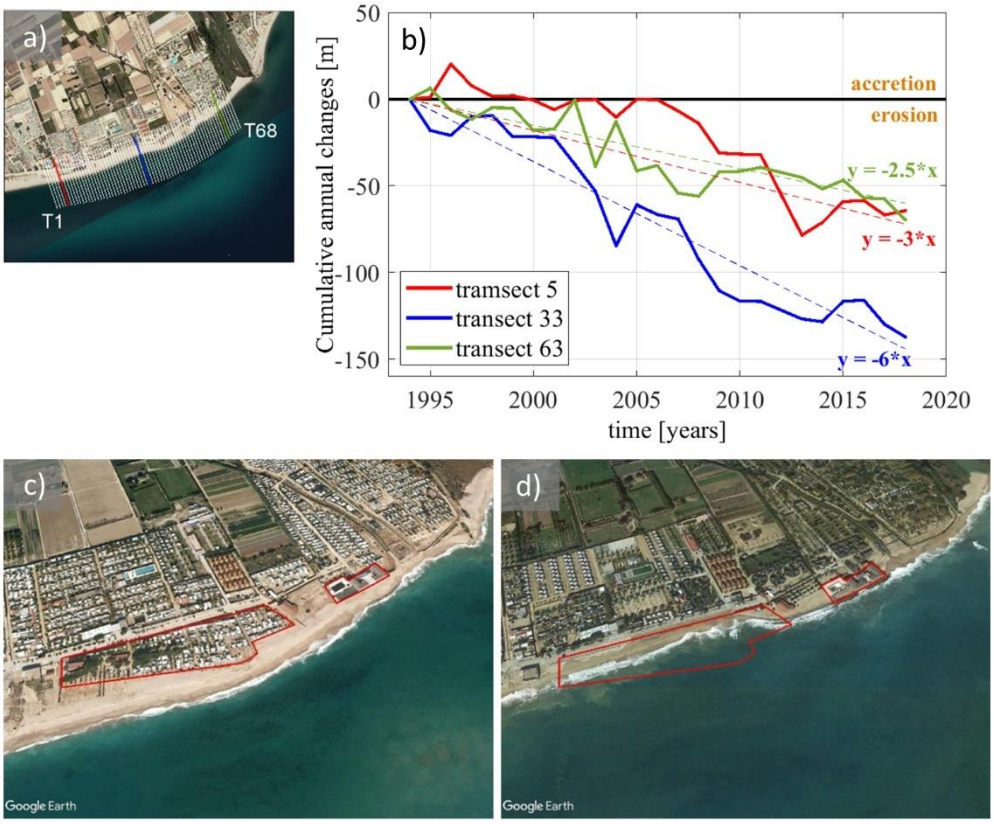

Figure 7: Long-term assessment in Malgrat Beach (Tordera Delta): a) cross-shore transects, b) long-term trends obtained at three profiles and beach erosion from c) 2007 to d) 2017. The red rectangle highlights structures affected by the erosion process.

These shoreline variation rates agree with values presented by Blasco (2011), who used high-resolution aerial photographs and obtained an average erosion rate of 4.68 m/year between 1995 and 2009 on the coast southward of the Tordera River mouth, a value similar to that obtained here using SDS (4.79 m/year) for the same period at the same location.

5.3.2. Short-term shoreline changes in Malgrat Beach (Tordera Delta): detection of nourishment and erosion events

In May 2015, a nourishment project was carried out to restore the beach and overcome the continuous erosion of Malgrat Beach. In November of the same year, a storm event hit the area, and a significant amount of the renourished sand was lost. The comparison of the SDSs obtained immediately before and immediately after each event (Figure 13) enabled the assessment of the evolution of the coast during that sequence of events. After the nourishment, the SDS advanced a maximum distance of approximately 60 m seaward, which is in agreement with the nourishment project records. Nevertheless, the analysis of the SDS after the storm event revealed a net seaward shift of only approximately 15 m (averaged along the beach) and net erosion on the northern section of the beach, with a landward retreat of more than 30 m caused by the storm.

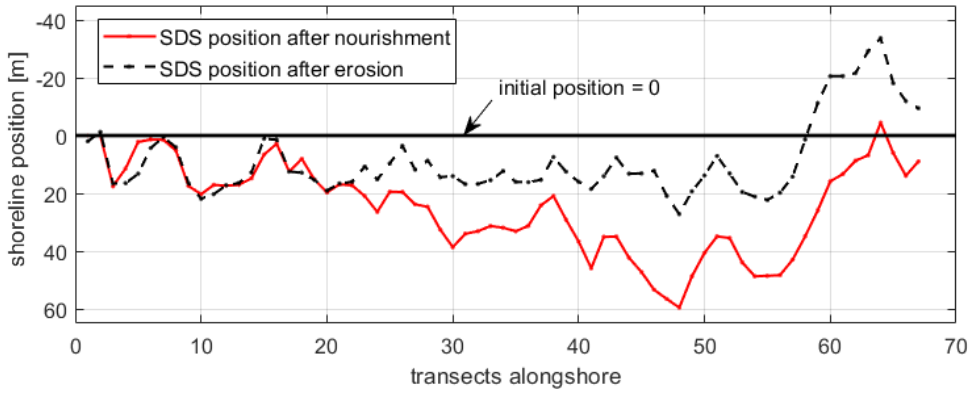

Figure 8: Short-term changes in Todera's shoreline after nourishment in May 2015 (red line) and after the storm event in November 2015 (black). The shoreline position refers to the SDS position before nourishment, with negative values indicating erosion and positive values indicating accretion. Cross-shore transects are the same as presented in Figure 12.

5.3.3. Changes in coastal bathymetry in Barcelona

The ability to detect the change in seabed morphology using SDBs in Barcelona before and after sediment backpassing in 2017 was assessed using the Brier skill score (BSS). The obtained BSS of 0.26 indicates that only part of the changes in the depth values due to backpassing is captured by the satellite data. This suggests that the errors in seabed changes detected with satellite-derived data are still high in comparison to the changes observed in situ (Figure 14).

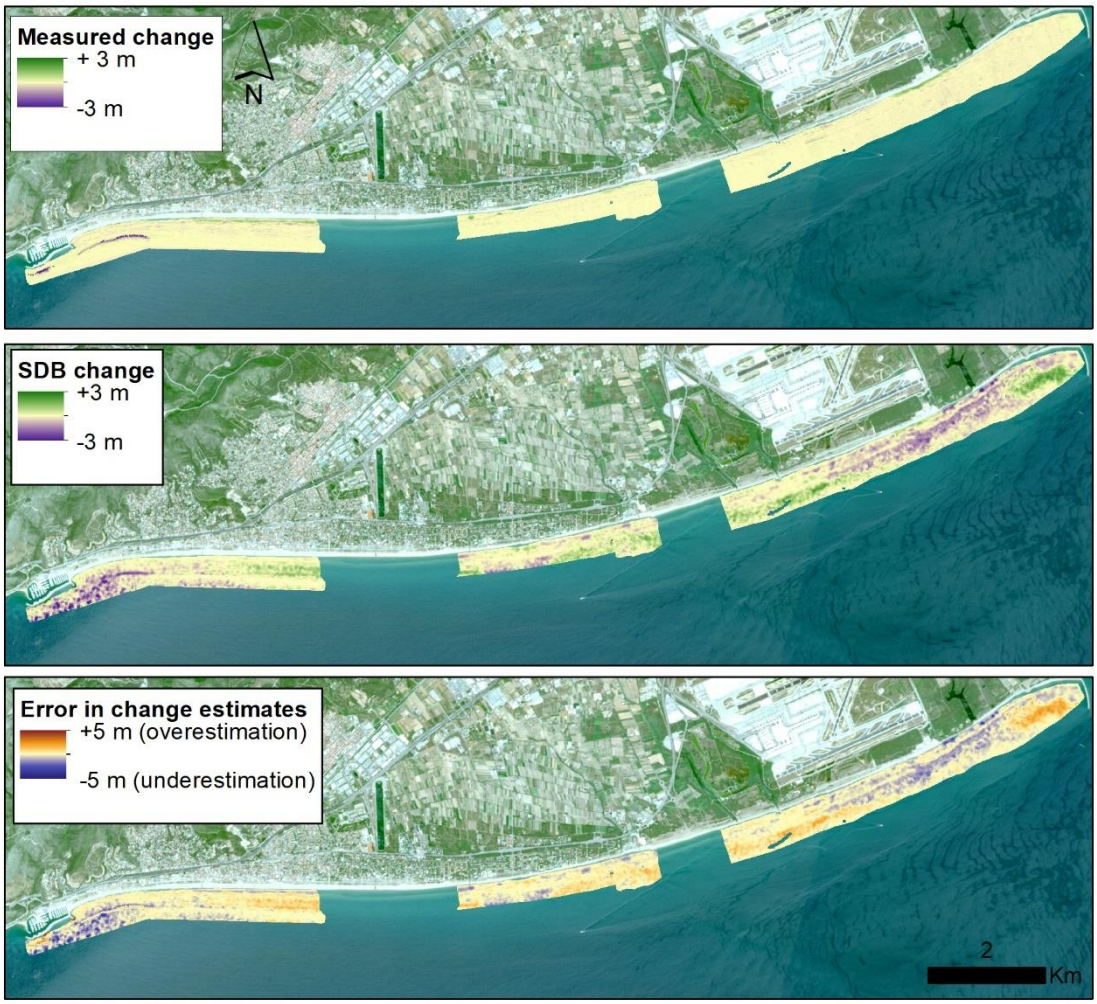

469

470 *Figure 14: Seabed changes detected from a)* in situ *measurements and b) SDB and c) the error between both*
471 *estimates.*

472 *5.3.4. Mid-term shoreline changes between Castellon and Sagunto Ports: seasonal beach*
473 *rotation*

474 A seasonal change in shoreline orientation was verified in three embayed beaches located
475 between Castellon and Sagunto Ports using heatmaps of SDSs from the summer of 2017 to the
476 winter of 2018 and from the winter of 2018 to the summer of 2018 (Figure 15). On these three
477 beaches, northeast waves approach the coast during the winter, driving southward longshore
478 sediment transport, whereas wave direction shifts to the southeast in the summer, which drives
479 sediments northward. That seasonal shift in wave patterns and beach rotation was reported
480 previously on the Spanish Eastern Mediterranean coast (e.g., Castelle et al., 2020; Ojeda and
481 Guillén, 2008; Turki et al., 2013), although the lack of in situ measurements did not allow a
482 quantitative assessment in this case.

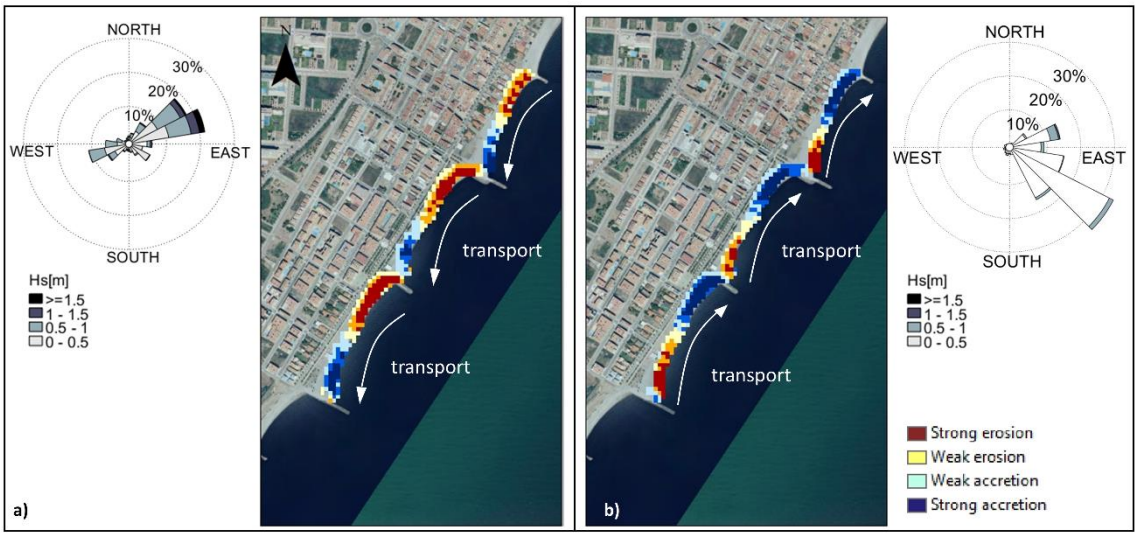

Figure 15: Seasonal beach rotation in beaches between Castellon and Sagunto Ports. a) Shoreline changes observed in the winter of 2018: shoreline erosion in the north and accretion southwards due to predominant northeast waves during winter. b) Shoreline changes observed in the summer of 2018: shoreline accretion in the north and erosion southwards due to predominant southeast waves during summer.

5.3.5. Long-term changes at the regional scale: identifying erosion hotspots in the Gulf of Cadiz

Erosion/accretion rates in cross-shore profiles (every 200 m) along the whole Gulf of Cadiz were obtained using SDSs from Landsat and Sentinel missions between 1995 and 2019 (Figure 16), which enabled the identification of erosion and accretion hotspots, as discussed here.

- The SDS analysis revealed that Punta del Montijo (Figure 15d) and Los Toruños Spit (Figure 16e) are the most critical areas in the province of Cadiz, which is in agreement with the findings of MITECO (2019), who identified these beaches, along with La Victoria Beach (Figure 16f), as areas under high erosion in previous studies:

    - At Punta del Montijo (Figure 16d), traditional aquiculture rubble-mound structures facilitate the updrift accumulation of sediment and the consequent downdrift erosion. Government and private initiatives built seawalls along the coast in this area, but these measures did not prevent erosion from occurring, according to previous studies.

    - The southern part of Los Toruños Spit is a naturally dynamic estuarine area, and significant erosion rates were observed in previous studies, whereas Valdelagrana (northward of Los Toruños) is a densely populated area where a seawall stabilizes the shoreline position (Figure 16e).

505 - The SDS analysis yielded a moderate erosion rate at La Victoria Beach. Erosion
506 in this area is partially related to the construction of groins to stabilize Santa
507 María del Mar Beach, located northwards of La Victoria Beach (Figure 16f).
508 These structures block northward longshore drift, causing erosion in La Victoria
509 and southward erosion at El Chato Beach (Figure 16f). However, this area is
510 constantly renourished with sand, which hampers our ability to identify erosion
511 problems using SDS analysis.

512 - The SDS analysis revealed Islantilla (Figure 16a) and Matalascañas (Figure 16c) as coastal
513 erosion hotspots in the province of Huelva, in agreement with CEDEX (2013), who stated
514 that these beaches are areas of critical erosion in which the reduction in the beach width
515 exposes the backshore during storm wave conditions.
516 - There is also coherence regarding areas that present shoreline accretion: CEDEX (2013)
517 reported a seaward shift of the shoreline in the updrift of Mazagon Port, and the same
518 pattern was verified here using SDS analysis (Figure 16b).

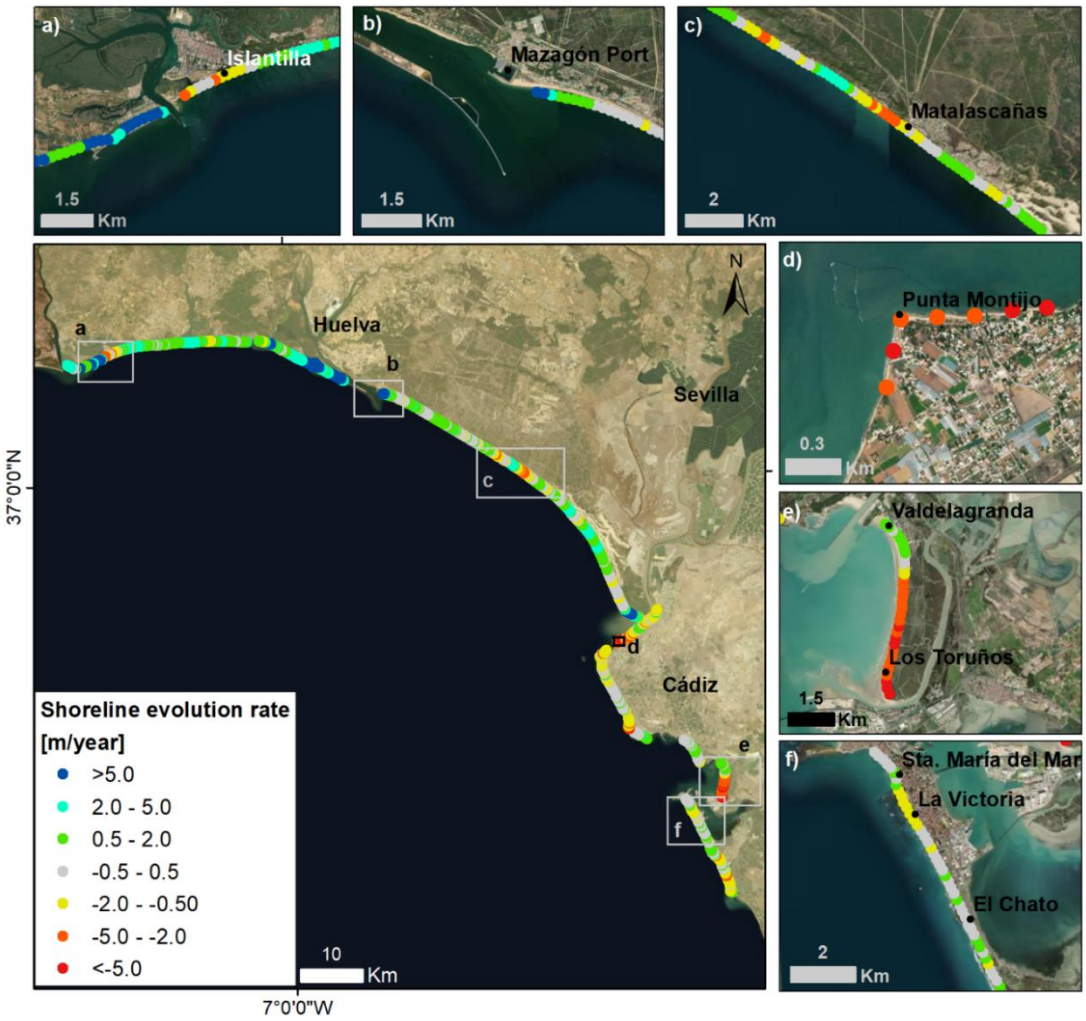

Figure 16: Long-term shoreline evolution rate along the Gulf of Cadiz. Negative (positive) values indicate erosive (accretive) trends. In detail, an example of areas where critical erosive/accretive trends were verified on the Huelva (a, b and c) and Cadiz (d, e, and f) coasts.

6. DISCUSSION

The results detailed in the previous section show that CEFS products can be used to detect changes at several temporal and spatial scales. A key point to reach the required accuracy and skill is the use of site-specific information within the processors (see Section 3.1). These results are discussed here, highlighting the strengths and weaknesses of these new developments.

6.1. Accuracy of CEFS products

The 1D products assessed here (SDWs and SWSs) presented positional errors (offsets) lower than the pixel size. Several sources of inaccuracies may contribute to the remaining offset, such as the resolution of satellite images and the SDW extraction process. The processor used to develop SDWs defines the waterline as the border of the pixels at the boundary between sea and land; thus, some positional error may occur if the waterline measured in situ is located inside the pixel. In this case, the positional accuracy depends on the pixel size, and further

improvements may be achieved with higher resolution images from future EO missions (Turner et al., 2021). To overcome this issue in current missions, some studies have suggested the use of interpolation techniques to obtain SDWs inside pixels. (Vos et al., 2019b) applied such an approach to increase the resolution of Landsat and Sentinel SDWs and obtained an overall RMSE lower than 13 m. Nevertheless, it is not clear whether these methods enhance the accuracy of satellite data. For example, Hagenaars et al. (2018) tested the use of interpolation methods to increase the resolution of SDWs, expecting to obtain higher accuracy from those products, but contrary to expectations, their results showed an increase in the offset value on the order of pixel size. No subpixel interpolation technique was applied in the development of the CEFS products, and it is remarkable that the estimated errors were approximately half of the pixel size.

Another source of inaccuracy may be related to the water level associated with SDWs. The nearshore water level at a specific time is the result of the combined effect of astronomical tides, storm surges, and short-term sea-level changes induced by breaking waves. While tide and surge levels can be obtained from tide gauge measurements, the complexity of the runup processes (including wave setup, infragravity surf beat, and swash) hampers the estimation of the exact runup level at the moment when the satellite image is taken. To account for the water level induced by waves, Castelle et al. (2021) suggested the use of mean runup (setup) or maximum runup (setup plus swash maximum) during a sea state, which can be estimated from empirical formulas (e.g., Stockdon et al., 2006) . In their pilot site, the water level that resulted in higher SDW accuracy was runup maxima, which is the maximum level reached by wave bores at the beach face. This choice makes sense when waterlines are detected at the wet-dry sand interface, and Castelle et al. (2021) acknowledged that it can render an overestimation of the water level associated with images taken during the downrush phase of swash, especially if waterlines are detected at the water-sand interface. For the development of the CEFS products assessed here, considering the mean and maximum runup in the estimation of the water level associated with SDWs worsened the accuracy of the SDWs (errors increased by a factor of 2 when using the mean and maximum runup). Therefore, sea-level changes induced by breaking waves were disregarded in the estimation of nearshore sea level.

Finally, some inaccuracies can be related to the beach slope used to transform SDWs into SDSs. The slope of the beach profile changes significantly along the beach and throughout the year due to seasonal variability in the marine climate. It can also present severe variations after extreme storm events or due to human actions. Slope data are estimated from sparse datasets often unavailable for the total extent of the target area or the total period under investigation.

An alternative to high-frequency in situ topographies is to use the time series of SDWs and the respective water levels to estimate the beach face topography in a certain time period. For example, using that approach, Vos et al. (2020) developed a tool to derive the beach slope from satellite images, which allows obtaining SDSs without requiring local topography.

6.2. Skill of CEFS products to detect changes

Coastal change processes at different temporal and spatial scales, such as seasonal and event-driven changes at local scale in Castellon-Sagunto and Tordera or at regional scales in the Gulf of Cadiz were verified from the coregistered time series of the CEFS products. However, cloud cover affects the sampling frequency of time series and limits the analyses of seasonal and short-term (storm) processes. The former depends on high-frequency time series, and the latter depends on the availability of satellite data on specific dates of interest. This is in accordance with the results presented by Vos et al. (2019b), who stated that intra-annual changes are barely detected by publicly available satellite data.

6.3. The importance of site-specific information

The CEFS products were developed on the basis that site-specific information is crucial to obtain reliable change assessments from satellite data. Thus, local characteristics were included in several phases of the products' development:

- In the coregistration phase, very high-resolution images from commercial missions were used as a reference to correct the geolocation of public images. For each site, a VHR image was used.

- In the detection phase, several spectral indices were tested (i.e., NDVI, GNDVI, NDWI) at each pilot site to guarantee reliable SDW identification.

- Finally, auxiliary data such as in situ measurements of the beach topography were used to obtain SDSs and to estimate the SDBs.

The need for site-specific input feeds the debate on whether automated satellite detection can be extrapolated to other sites and spatial scales. Recent methods and tools that provide automatic SDW and SDS change rates (based on single-slope and water level records) (e.g., Almeida et al., 2021; Hagenaars et al., 2018; Vos et al., 2019b) have been shown to be useful and have been widely applied by the coastal community. Site-specific information is used to obtain the SDS change rates in those tools, but the SDW processor is usually calibrated with data from a few beaches (micro and mesotidal); thus, the reliability of the results may not be even at

all sites, especially at those sites with characteristics that differ from calibration (Castelle et al., 2021; Ceccon et al., 2021). As an example, the same spectral index is used in most of those waterline detection tools; however, the analysis in Spain with different spectral indices (i.e., NDVI, GNDVI, NDWI) showed that some indices work better than others according to local conditions.

The need for auxiliary data to enhance the accuracy and skill of CEFS products limits the benefit of replacing in situ measurements with satellite data in current monitoring practices. However, the amount of in situ measurements needed to obtain high-quality satellite products was significantly lower than the in-situ measurements required for the traditional monitoring methods, and such a transition from in situ measurements to satellite data undoubtedly reduces the cost of monitoring activities.

6.3. Future outreach

Great advances have been made in recent years regarding Earth observation. However, further research is still recommended to refine coastal change detection from satellite images. An extension of the CEFS project (completed in March 2021) commenced in June 2021 under the name “Coastal Evolution from Space” (to be completed in May 2022), and here, we highlight some of the planned future research:

- Here, the detection of beach SDWs was based on the water-sand interface. The detection of coastlines based on other proxies, such as the vegetation line, scarp edges, the top of the cliffs, or the boundary with backshore structures, is to be investigated to allow coastal change detection for the monitoring of other environments, such as cliffs, sand dunes, and urban areas.
- The CEFS project explored 2D products (land cover maps), but they were not applied to assess coastal erosion processes in the Spanish pilot sites presented in this work. Time series of 2D products are to be developed in future works for the assessment of coastal changes not explored here, such as changes in the dune vegetation that affect dune morphology and the ecosystem services provided by the dune to coastal systems.
- More studies are necessary to investigate the best estimation of the instantaneous water level related to SDWs and the automated computation of the beach face slope to improve the transformation of SDWs into datum-based SDSs (see Section 6.1).
- Further research is also required to improve the sampling frequency of satellite time series, which will allow coastal change analyses at scales that are not currently assessed. Earth observation by means of synthetic aperture radar (SAR) sensors might overcome

some of the limitations of optical sensors because they do not depend on sunlight and penetrate cloud cover. Furthermore, the improvement in frequency sampling that SAR can provide to SDW time series will be a key contribution to the stochastic analysis of shoreline changes. The possibility of using optical and SAR sensors deployed in current satellite missions to build high-frequency coregistered time series is promising (Costantini et al., 2018; Hnatushenko et al., 2021; Ye et al., 2021). However, because of the distinct nature of SAR and optical images, shoreline detection is different, and further research is still necessary to obtain accurate SAR shorelines and compose reliable time series. First, the verification of SAR-derived products requires an expert since regular visual checks are not possible, whereas optical images are more familiar to nonexperts than SAR images. Second, the positioning accuracy of SAR products depends on the angle of measurement and on the satellite trajectory (ascending/descending), which requires further investigation.

7. CONCLUSIONS

This work focused on assessing the capability to monitor changes in coastal morphology at various temporal and spatial scales, making use of satellite-derived data obtained from site-specific processing methods, such as CEFS products. The results of the products' accuracy analysis indicated high horizontal accuracy, with errors on the order of half of the pixel size. Some in situ measurements are necessary to obtain satellite data that represent site-specific conditions. However, the quantity of required data measured in situ is significantly lower than the quantity required by traditional monitoring methods.

Time-series analysis with SDW and SDS products showed that coastal change processes can be detected at several temporal and spatial scales, such as short-term erosion and accretion events on a small beach, seasonal beach rotation, and long-term trends at local and regional scales. The results from SDBs indicated that the quantitative assessment of the coastal morphology with these 3D products is still limited. The analysis of SDB from Barcelona showed that in some areas of high suspended sediment concentration, it is possible to generate quality bathymetry under certain conditions. However, for some coastal monitoring practices, higher accuracy in detecting seabed changes and a higher sampling frequency is still necessary. At present, the accuracy that can be achieved by remote sensing techniques to detect the seabed is still not enough to afford the full shift from the use of in situ measurements to satellite-derived products. Generally, the sediment concentration in the water is still a challenge to obtain satellite-derived bathymetry

from optical sensors, and further research on methods to obtain SDBs in these challenging areas is clearly necessary.

The CEFS project brought together experts with different backgrounds, such as Earth observation and coastal engineering and management. The satellite-derived data used in this work benefit from the site-specific approach of the methods applied to extract relevant information from satellite imagery to monitor changes in coastal morphology and overcome one of the critical issues of general tools. An important advance of the satellite dataset used here is that it is based on coregistered images that guarantee precision between images from different missions and allows change analyses at different temporal resolutions. Although this approach has been widely used to assess environmental changes from satellites in other thematic areas (e.g., Cucchiaro et al., 2020; Nuth and Kääb, 2011), it is still little explored for assessing changes in coastal morphology.

It is important to remark that the accuracy of satellite products is greatly limited by the spatial resolution, and improvements are expected with higher resolution Earth observation data from future missions. Further improvements are also expected regarding the sampling frequency of the satellite time series obtained from optical sensors, which is not enough to represent some short-term processes. The development of coregistered multiple-sensor (SAR and optical, for example) time series is promising and can overcome that issue. Because of the distinct natures of SAR and optical images, shoreline detection is different, and more studies on that topic are still necessary to achieve reliable composite time series.

Further investigations are already ongoing in the framework of the extension of the CEFS project, under the name of the “Coastal Evolution From Space” project.

8. ACKNOWLEDGMENTS

This work was financially supported by the Coastal Erosion Project – ESA. The Coastal Erosion Project is funded via the Science for Society slice of the 5th Earth Observation Envelope Program (EOEP-5) of the European Space Agency.

The authors are very thankful to the Coastal Change Consortium, a partnership bringing together the delivery of products team, comprising ARGANS Ltd, IsardSAT & AdwaisEO, and the user group comprising IH Cantabria, the British Geological Survey, Geological Survey of Ireland, and Arctus in collaboration with the University of Quebec at Rimouski. Special thanks are also given to Ana García Fletcher and Roberto Díaz Sánchez from the Ministry for the Ecological Transition and the Demographic Challenge (MITECO) and to the broad end-user community, including the

Barcelona Port Authority, the National Geographic Institute (IGN), the Spanish Navy Hydrographic Institute (IHM), the Polytechnic University of Catalonia (UPC), the Polytechnic University of Valencia (UPV), AZTI, for providing the auxiliary data used in product development and validation and for valuable insights and discussions on what Spanish end-users need from satellite-derived products. Finally, we thank Puertos del Estado and IHCantabria for providing the oceanographic data used in product development.

9. REFERENCES

Almeida, L.P., Efraim de Oliveira, I., Lyra, R., Scaranto Dazzi, R.L., Martins, V.G., Henrique da Fontoura Klein, A., 2021. Coastal Analyst System from Space Imagery Engine (CASSIE): Shoreline management module. Environ. Model. Softw. 140. https://doi.org/10.1016/j.envsoft.2021.105033

Blasco, D., 2011. Evolución costera del maresme norte (Blanes-Arenys). Universitat Politècnica de Catalunya.

Caballero, I., Stumpf, R., 2020. Towards Routine Mapping of Shallow Bathymetry in Environments with Variable Turbidity: Contribution of Sentinel-2A/B Satellites Mission. Remote Sens. 12. https://doi.org/10.3390/rs12030451

Caballero, I., Stumpf, R.P., 2021. On the use of Sentinel-2 satellites and lidar surveys for the change detection of shallow bathymetry: The case study of North Carolina inlets. Coast. Eng. 169. https://doi.org/10.1016/j.coastaleng.2021.103936

Castelle, B., Masselink, G., Scott, T., Stokes, C., Konstantinou, A., Marieu, V., Bujan, S., 2021. Satellite-derived shoreline detection at a high-energy meso-macrotidal beach. Geomorphology 383. https://doi.org/10.1016/j.geomorph.2021.107707

Castelle, B., Robinet, A., Idier, D., D'Anna, M., 2020. Modelling of embayed beach equilibrium planform and rotation signal. Geomorphology 369. https://doi.org/10.1016/j.geomorph.2020.107367

Ceccon, P.E.S., Ciavola, P., Armaroli, C., 2021. Performance of remote sensing algorithms for shoreline mapping under different beach morphodynamic conditions, in: EGU General Assembly 2021. Vienna. https://doi.org/10.5194/egusphere-egu21-13028

CEDEX, 2013. Estudio de la dinámica litoral, defensa y propuesta de mejora en las playas con problemas: Estudio de actuación del tramo de costa comprendido entre las

desembocaduras de los ríos Guadiana y Guadalquivir.

Cid, A., Castanedo, S., Abascal, A.J., Menéndez, M., Medina, R., 2014. A high resolution hindcast of the meteorological sea level component for Southern Europe: the GOS dataset. Clim. Dyn. 43, 2167–2184. https://doi.org/10.1007/s00382-013-2041-0

Clerc, S., 2021. S2 MPC - L1C data quality report.

Cooper, J.A.G., Masselink, G., Coco, G., Short, A.D., Castelle, B., Rogers, K., Anthony, E., Green, A.N., Kelley, J.T., Pilkey, O.H., Jackson, D.W.T., 2020. Sandy beaches can survive sea-level rise. Nat. Clim. Chang. 10, 993–995. https://doi.org/10.1038/s41558-020-00934-2

Costantini, M., Zavagli, M., Martin, J., Medina, A., Barghini, A., Naya, J., Hernando, C., Macina, F., Ruiz, I., Nicolas, E., Fernandez, S., 2018. Automatic Coregistration of SAR and Optical Images Exploiting Complementary Geometry and Mutual Information, in: IGARSS 2018 - 2018 IEEE International Geoscience and Remote Sensing Symposium. IEEE, Valencia, pp. 8877–8880. https://doi.org/10.1109/IGARSS.2018.8519242

Cucchiaro, S., Maset, E., Cavalli, M., Crema, S., Marchi, L., Beinat, A., Cazorzi, F., 2020. How does co-registration affect geomorphic change estimates in multi-temporal surveys? GIScience Remote Sens. 57. https://doi.org/10.1080/15481603.2020.1763048

Erena, M., Domínguez, J.A., Atenza, J.F., García-Galiano, S., Soria, J., Pérez-Ruzafa, Á., 2020. Bathymetry Time Series Using High Spatial Resolution Satellite Images. Water 12. https://doi.org/10.3390/w12020531

Françoise, B., Pau, E., Eulàlia, M., 2000. Rehabilitation of metropolitan beaches by local administrations in Catalonia: new trends in sustainable coastal management. J. Coast. Conserv. 6, 97–106. https://doi.org/10.1007/BF02730473

Gao, B., 1996. NDWI—A normalized difference water index for remote sensing of vegetation liquid water from space. Remote Sens. Environ. 58, 257–266. https://doi.org/10.1016/S0034-4257(96)00067-3

Gitelson, A.A., Kaufman, Y.J., Merzlyak, M.N., 1996. Use of a green channel in remote sensing of global vegetation from EOS- MODIS. Remote Sens. Environ. 58, 289–298. https://doi.org/10.1016/S0034-4257(96)00072-7

Gomes da Silva, P., Beck, A.-L., Martinez Sanchez, J., Medina Santanmaria, R., Jones, M., Taji, A., 2020. Advances on coastal erosion assessment from satellite earth observations: exploring the use of Sentinel products along with very high resolution sensors, in: Edited

759 by: Bonora, L.; Carboni, D.; De Vincenzi, M. (Ed.), Eighth International Symposium
760 “Monitoring of Mediterranean Coastal Areas. Problems and Measurement Techniques.”
761 Firenze Firenze University Press, Livorno (Italy), pp. 412–421.
762 https://doi.org/10.36253/978-88-5518-147-1.41

763 Gorelick, N., Hancher, M., Dixon, M., Ilyushchenko, S., Thau, D., Moore, R., 2017. Google Earth
764 Engine: Planetary-scale geospatial analysis for everyone. Remote Sens. Environ. 202, 18–
765 27. https://doi.org/10.1016/j.rse.2017.06.031

766 Hagenaars, G., de Vries, S., Luijendijk, A.P., de Boer, W.P., Reniers, A.J.H.M., 2018. On the
767 accuracy of automated shoreline detection derived from satellite imagery: A case study
768 of the sand motor mega-scale nourishment. Coast. Eng. 133, 113–125.
769 https://doi.org/10.1016/j.coastaleng.2017.12.011

770 Himmelstoss, E.A., Henderson, R.E., Kratzmann, M.G., Farris, A.S., 2018. No Title, Open-File
771 Report 2018-1179. https://doi.org/https://doi.org/10.3133/ofr20181179

772 Hnatushenko, V., Kogut, P., Uvarov, M., 2021. On Flexible Co-registration of Optical and SAR
773 Satellite Images, in: Babichev, S., Lytvynenko, V., Wójcik, W., Vyshemyrskaya, S. (Eds.),
774 Advances in Inteligent Systems and Computing. Springer, pp. 515–534.
775 https://doi.org/10.1007/978-3-030-54215-3_33

776 Jiménez, J.A., Gracia, V., Valdemoro, H.I., Mendoza, E.T., Sánchez-Arcilla, A., 2011. Managing
777 erosion-induced problems in NW Mediterranean urban beaches. Ocean Coast. Manag.
778 54, 907–918. https://doi.org/10.1016/j.ocecoaman.2011.05.003

779 Jiménez, J.A., Sanuy, M., Ballesteros, C., Valdemoro, H.I., 2018. The Tordera Delta, a hotspot to
780 storm impacts in the coast northwards of Barcelona (NW Mediterranean). Coast. Eng.
781 134, 148–158. https://doi.org/10.1016/j.coastaleng.2017.08.012

782 Luijendijk, A., Hagenaars, G., Ranasinghe, R., Baart, F., Donchyts, G., Aarninkhof, S., 2018. The
783 State of the World’s Beaches. Sci. Rep. 8. https://doi.org/10.1038/s41598-018-24630-6

784 MITECO, 2019. Estrategias para la protección costera en las provincias de Cádiz, Málaga y
785 Almería considerando los efectos del cambio climático.

786 Nuth, C., Kääb, A., 2011. Co-registration and bias corrections of satellite elevation data sets for
787 quantifying glacier thickness change. Cryosph. 5, 271–290. https://doi.org/10.5194/tc-5-
788 271-2011

789 Ojeda, E., Guillén, J., 2008. Shoreline dynamics and beach rotation of artificial embayed

790 beaches. Mar. Geol. 253, 51–62. https://doi.org/10.1016/j.margeo.2008.03.010

791 Ruggiero, P., Kaminsky, G.M., Gelfenbaum, G., 2003. Linking Proxy-Based and Datum-Based
792 Shorelines on a High-Energy Coastline: Implications for Shoreline Change Analyses. J.
793 Coast. Res. 57–82.

794 Ruiz-Luna, A., Berlanga-Robles, C.A., 2003. Land use, land cover changes and coastal lagoon
795 surface reduction associated with urban growth in northwest Mexico. Landsc. Ecol. 18,
796 159–171. https://doi.org/10.1023/A:1024461215456

797 Sanuy, M., Jiménez, J.A., 2019. Sensitivity of Storm-Induced Hazards in a Highly Curvilinear
798 Coastline to Changing Storm Directions. The Tordera Delta Case (NW Mediterranean).
799 Water 11. https://doi.org/10.3390/w11040747

800 Stockdon, H.F., Holman, R.A., Howd, P.A., Sallenger, A.H., 2006. Empirical parameterization of
801 setup, swash, and runup. Coast. Eng. 53, 573–588.
802 https://doi.org/10.1016/j.coastaleng.2005.12.005

803 Sutherland, J., Peet, A.H., Soulsby, R.L., 2004. Evaluating the performance of morphological
804 models. Coast. Eng. 51, 917–939. https://doi.org/10.1016/j.coastaleng.2004.07.015

805 Tarpley, J.D., Schneider, S.R., Money, R.L., 1984. Global Vegetation Indices from the NOAA-7
806 Meteorological Satellite. J. Clim. Appl. Meteorol. 23, 491–494.
807 https://doi.org/10.1175/1520-0450(1984)023<0491:GVIFTN>2.0.CO;2

808 Turki, I., Medina, R., Coco, G., Gonzalez, M., 2013. An equilibrium model to predict shoreline
809 rotation of pocket beaches. Mar. Geol. 346, 220–232.
810 https://doi.org/10.1016/j.margeo.2013.08.002

811 Turner, I.L., Harley, M.D., Almar, R., Bergsma, E.W.J., 2021. Satellite optical imagery in Coastal
812 Engineering. Coast. Eng. 167. https://doi.org/10.1016/j.coastaleng.2021.103919

813 Vieira Da Silva, G., Muler, M., Prado, M.F.V., Short, A.D., Henrique da Fontoura Klein, A., Toldo,
814 E.E., 2016. Shoreline Change Analysis and Insight into the Sediment Transport Path along
815 Santa Catarina Island North Shore, Brazil. J. Coast. Res. 32, 863–874.
816 https://doi.org/10.2112/JCOASTRES-D-15-00164.1

817 Vos, K., Harley, M.D., Splinter, K.D., Simmons, J.A., Turner, I.L., 2019a. Sub-annual to multi-
818 decadal shoreline variability from publicly available satellite imagery. Coast. Eng. 150,
819 160–174. https://doi.org/10.1016/j.coastaleng.2019.04.004

Vos, K., Harley, M.D., Splinter, K.D., Walker, A., Turner, I.L., 2020. Beach Slopes From Satellite-Derived Shorelines. Geophys. Res. Lett. 47. https://doi.org/10.1029/2020GL088365

Vos, K., Splinter, K.D., Harley, M.D., Simmons, J.A., Turner, I.L., 2019b. CoastSat: A Google Earth Engine-enabled Python toolkit to extract shorelines from publicly available satellite imagery. Environ. Model. Softw. 122. https://doi.org/10.1016/j.envsoft.2019.104528

Vousdoukas, M.I., Ranasinghe, R., Mentaschi, L., Plomaritis, T.A., Athanasiou, P., Luijendijk, A., Feyen, L., 2020a. Sandy coastlines under threat of erosion. Nat. Clim. Chang. 10, 260–263. https://doi.org/10.1038/s41558-020-0697-0

Vousdoukas, M.I., Ranasinghe, R., Mentaschi, L., Plomaritis, T.A., Athanasiou, P., Luijendijk, A., Feyen, L., 2020b. Reply to: Sandy beaches can survive sea-level rise. Nat. Clim. Chang. 10, 996–997. https://doi.org/10.1038/s41558-020-00935-1

Wang, Z., Bovik, A.C., Sheikh, H.R., Simoncelli, E.P., 2004. Image Quality Assessment: From Error Visibility to Structural Similarity. IEEE Trans. Image Process. 13, 600–612. https://doi.org/10.1109/TIP.2003.819861

Ye, Y., Yang, C., Zhu, B., Zhou, L., He, Y., Jia, H., 2021. Improving Co-Registration for Sentinel-1 SAR and Sentinel-2 Optical Images. Remote Sens. 13, 928. https://doi.org/10.3390/rs13050928

Yunus, A.P., Dou, J., Song, X., Avtar, R., 2019. Improved Bathymetric Mapping of Coastal and Lake Environments Using Sentinel-2 and Landsat-8 Images. Sensors 19, 2788. https://doi.org/10.3390/s19122788